Assimilation of Simulated Polarimetric Radar Data for a Convective Storm Using the Ensemble Kalman Filter. Part II: Impact of Polarimetric Data on Storm Analysis

YOUNGSUN JUNG AND MING XUE

School of Meteorology, and Center for Analysis and Prediction of Storms, University of Oklahoma, Norman, Oklahoma

GUIFU ZHANG AND JERRY M. STRAKA

School of Meteorology, University of Oklahoma, Norman, Oklahoma

(Manuscript received 22 June 2007, in final form 20 November 2007)

ABSTRACT

A data assimilation system based on the ensemble square-root Kalman filter (EnSRF) is extended to include the additional capability of assimilating polarimetric radar variables. It is used to assess the impact of assimilating additional polarimetric observations on convective storm analysis in the Observing System Simulation Experiment (OSSE) framework. The polarimetric variables considered include differential reflectivity Z_{DR}, reflectivity difference Z_{dp}, and specific differential phase K_{DP}. To simulate the observational data more realistically, a new error model is introduced for characterizing the errors of the nonpolarimetric and polarimetric radar variables. The error model includes both correlated and uncorrelated error components for reflectivities at horizontal and vertical polarizations (Z_H and Z_V, respectively). It is shown that the storm analysis is improved when polarimetric variables are assimilated in addition to Z_H or in addition to both Z_H and radial velocity V_r. Positive impact is largest when Z_{DR}, Z_{dp}, and K_{DP} are assimilated all together. Improvement is generally larger in vertical velocity, water vapor, and rainwater mixing ratios. The rainwater field benefits the most while the impacts on horizontal wind components and snow mixing ratio are smaller. Improvement is found at all model levels even though the polarimetric data, after the application of thresholds, are mostly limited to the lower levels. Among Z_{DR}, Z_{dp}, and K_{DP}, Z_{DR} is found to produce the largest positive impact on the analysis. It is suggested that Z_{DR} provides more independent information than the other variables. The impact of polarimetric data is also expected to be larger when they are used to retrieve drop size distribution parameters. The polarimetric radar data thresholding prior to assimilation is found to be necessary to minimize the impact of noise. This study is believed to be the first to *directly* assimilate (simulated) polarimetric data into a numerical model.

1. Introduction

For convective-scale NWP, microphysics represents perhaps one of the most important physical processes with both direct and indirect influences. The microphysical processes depend to a large extent on the phase, density, and the drop size distributions (DSDs) of the microphysical species involved. These properties also directly affect radar measurements within each radar sampling volume. For these reasons, equivalent radar reflectivity factor (hereinafter reflectivity) and radial velocity measurements from conventional Doppler weather radars are usually insufficient to fully describe the microphysical states in a convective storm. Additional observational parameters available from polarimetric Doppler radars, including differential reflectivity and differential phase measurements can be very helpful here as they contain information about the density, shape, and DSDs of hydrometeors (Doviak and Zrnic 1993; Bringi and Chandrasekar 2001).

The use of differential reflectivity for meteorological applications, in particular for rainfall estimation, was first proposed by Seliga and Bringi (1976); many studies have shown that polarimetric measurements can improve precipitation-type classification and quantitative rainfall estimates (Straka et al. 2000). Ryzhkov et al. (1998) and Vivekanandan et al. (1994) have proposed that polarimetric methods can estimate ice water content more accurately than the one that only uses reflec-

Corresponding author address: Ming Xue, Center for Analysis and Prediction of Storms, National Weather Center, Suite 2500, 120 David L. Boren Blvd., Norman, OK 73072.
E-mail: mxue@ou.edu

DOI: 10.1175/2007MWR2288.1

tivity (Z_H). Wu et al. (2000) used differential reflectivity (Z_{DR}) indirectly (rain and ice mixing ratios were derived from reflectivity and Z_{DR} before assimilation) in a cloud-scale four-dimensional variational data assimilation (4DVAR) system and obtained somewhat encouraging results. Moreover, the planned polarimetry upgrade starting later this decade or early next decade (D. Zrnic 2006, personal communication) by the National Weather Services (NWS) of the entire operational Weather Surveillance Radar-1988 Doppler (WSR-88D) radar network will undoubtedly motivate more active research on the utilization of polarimetric radar data.

An accurate estimate of the amounts of hydrometeors and DSDs using polarimetric radar data can contribute to the improvement and verification of microphysical parameterizations in cloud and mesoscale models. Such estimations can also help enhance our understanding of the interactions between microphysics and kinematics in severe storms and in the mesoscale system (Straka et al. 2000). Polarimetric radars also should be helpful for storm-scale model initialization, especially of the microphysical and related thermodynamic fields, through data assimilation.

The accuracy of NWP depends on the model initial condition. The error in the initial state grows with time and makes the predicted state diverge from its true state. Therefore, a lot of effort has been given to determining more accurate initial conditions that can lead to more accurate weather forecasts. Currently, the two most promising data assimilation techniques for obtaining the atmospheric initial condition or the best estimate of the atmospheric state are the 4DVAR (Le Dimet and Talagrand 1986; Courtier and Talagrand 1987) and the ensemble Kalman filter (EnKF) method (Evensen 1994; Evensen and Leeuwen 1996; Burgers et al. 1998; Houtekamer and Mitchell 1998; Anderson 2001; Bishop et al. 2001; Whitaker and Hamill 2002; Evensen 2003; Tippett et al. 2003), because of their ability to make effective use of the dynamic model equations and observations distributed in space and time, and to provide the best estimate that is also consistent with the prediction model. Because of its ability in handling complex, nonlinear, physical processes (e.g., ice microphysics) in the assimilation model, and in the forward observation operators (e.g., those for reflectivity), the EnKF method appears to be more suitable for convective-scale data assimilation, which is the main interest of our current study.

The EnKF technique was introduced into the meteorological community about a decade ago and has become very popular in recent years. It is an attractive alternative to the more mature 4DVAR method. Very encouraging results have been obtained by a number of researchers for large-scale models (e.g., Houtekamer et al. 2005; Whitaker et al. 2004). Tests with perfect prediction models with simulated Doppler radar data at the convective scale with EnKF have also produced very encouraging success in recent studies. The first paper to investigate the potential of EnKF for assimilating Doppler radar data was Snyder and Zhang (2003). The study used a cloud model with warm rain microphysics and assimilated simulated radial velocity data assumed to be available on the model grid. The studies of Tong and Xue (2005, hereinafter TX05) and Xue et al. (2006, hereinafter XTD06) further demonstrated that the cloud fields associated with a three-ice microphysics scheme (cloud ice, snow aggregates, and hail) can be accurately retrieved using the EnKF method. Moreover the inclusion of reflectivity data improves the results even though its observation operator is highly nonlinear. XTD06 also removed the assumption that radar data are available on the model grid and used more realistic radar-beam-pattern-based forward observation operators.

More recently, Tong and Xue (2008a,b, hereinafter TX08a and TX08b, respectively) applied the ensemble Kalman filter technique to the problem of simultaneous estimation of the atmospheric state of a convective storm and uncertain DSD-related microphysics parameters associated with a single-moment microphysics scheme, from radar radial velocity and reflectivity data. It was found that the parameter estimation can always be successful when only one of the parameters contains error. The difficulty of parameter estimation increases when multiple parameters contain error and have to be estimated simultaneously. The fact that the errors in some of the parameters produce compensating responses in terms of the observed radar reflectivity, causing solution nonuniqueness, is believed to be the reason for the difficulties. The study suggests that additional polarimetric radar measurements that provide the microphysics and DSD information can help alleviate the solution's nonuniqueness problem. Even when microphysics parameter estimation is not performed, the additional polarimetric measurements are expected to improve the microphysical state estimation. When the microphysics scheme predicts more than one moment (i.e., the mixing ratios), then more microphysical state variables (e.g., the total number concentration and reflectivity factor, as in the three-moment scheme of Milbrandt and Yau 2005) have to be estimated. If the radial velocity and conventional reflectivity are the only two storm-scale observations, the full state estimation is likely to be very difficult.

In this paper, we report on the results of our initial

efforts in developing capabilities to assimilate polarimetric radar data into a storm-scale NWP model, and in studying the impact of these variables on the analysis or model state estimation. We extended the ensemble Kalman filter data assimilation framework of TX05, XTD06, and TX08a, by adding the ability to assimilate the differential reflectivity ($Z_{\rm DR}$), reflectivity difference ($Z_{\rm dp}$), and specific differential phase ($K_{\rm DP}$). In Jung et al. (2008, hereinafter Part I), the development of the observational operators for these parameters are described, together with an examination of their applications to a simulated squall line and supercell storm. These observation operators are used in the EnKF Observing System Simulation Experiment (OSSE) system to produce the simulated observation and to assimilate the data. Other polarimetric parameters such as the correlation coefficient $\rho_{\rm hv}(0)$ can be added in the future.

In section 2, the simulation of the radar observations to be used in the OSSEs is discussed, together with their error models. The supercell simulation used in Part I is used as the truth simulation from which error-containing observations are generated. It is followed by the design and configurations of the OSSE data assimilation experiments. The impact of assimilating additional polarimetric variables is examined in section 3 based on the OSSE results. In section 4, we conclude our study and discuss some practical issues in the use of polarimetric radar data for data assimilation purposes. We believe the study reported herein represents the first attempt to *directly* assimilate polarimetric radar data into a numerical model.

2. Assimilation system and experimental design

The prediction model and the truth simulation of a supercell storm used for OSSEs are described in Part I. In the following, we first describe the simulation of the observations from this truth simulation and the error modeling for the reflectivity and polarimetric variables.

a. Simulation of observations and the error model

Real observations are usually contaminated by measurement and sampling errors, and can contain representativeness error also. In our radar simulator, error-free observations are first generated at model grid points using the observation operators developed in Part I, with the state variables of the truth simulation as input. The results are then brought to the radar elevation levels through interpolation and necessary beam-pattern weighting. We assume that the radar data are at the model grid columns, which is also an assumption made in XTD06. The effective earth radius model is used to take into account the effect of beam bending due to the surface curvature of the earth and the vertical change of the refractive index (Doviak and Zrnic 1993). A Gaussian beam weighting function described in XTD06 is used in the vertical direction to simulate Z_h, Z_v, V_r, and $K_{\rm DP}$ observations on the radar elevation planes.

Noise is then added to the error-free observations to simulate observation errors. Operational polarimetric WSR-88D radars transmit and receive horizontally and vertically polarized waves simultaneously, which measures Z_h and Z_v from the same pulses. Because the errors in Z_h and Z_v are mostly correlated for weather echoes in this configuration, the error in $Z_{\rm DR}$ is usually small because $Z_{\rm DR}$ is a ratio between Z_h and Z_v. To more realistically model the errors, correlated and uncorrelated random errors having Gaussian distributions are added to uncontaminated Z_h^t and Z_v^t in the linear domain (before the logarithmic transform) and converted to logarithmic reflectivity, Z_H and Z_V (Xue et al. 2007), so that

$$Z_H^o = 10\log_{10}(Z_h^t + \varepsilon_{\rm corr} + \varepsilon_h) \quad \text{and} \tag{1}$$

$$Z_V^o = 10\log_{10}(Z_v^t + \varepsilon_{\rm corr} + \varepsilon_v), \tag{2}$$

where superscripts t and o denote the uncontaminated (truth) and error-containing simulated observations, respectively. Here $\varepsilon_{\rm corr}$ represents the correlated part of the error and ε_h and ε_v are the uncorrelated errors for Z_h and Z_v, respectively. They are randomly generated Gaussian errors with zero means and standard deviations proportional to the (uncontaminated) reflectivity (Z_h), as real sampling errors should behave (Doviak and Zrnic 1993; Xue et al. 2007).

Briefly, the actual sizes of the standard deviation (hereafter effective error SD) of the error are experimentally determined in the following way. First, errors $\varepsilon_{\rm corr}$, ε_h, and ε_v are simulated by multiplying Z_h^t by a specified factor representing the relative error magnitude for each of them, and by a Gaussian-distributed random number with a zero mean and a standard deviation of one. The errors are then used in (1) and (2) to give Z_H^o and $Z_{\rm DR}^o$. These error-containing data are collected over the points where $Z_H^o > 0$ dBZ and $Z_{\rm DR}^o > 0$ dB, respectively, for all data sampling times; the effective error SD for each dataset are then calculated. To obtain desired levels of the SD of data for the purpose of data assimilation experiments, these steps are repeated through trials with different combinations of $\varepsilon_{\rm corr}$ and ε_h (and ε_v) until they are obtained. With this error model, errors are Gaussian distributed in the linear domain but become non-Gaussian when they are transformed to the log domain. For further details and

discussions on the error model, the reader is referred to Xue et al. (2007).

The observations of $Z^o_{\rm DR}$ and $Z^o_{\rm dp}$ are generated from Z^o_h and Z^o_v. The errors in $Z^o_{\rm DR}$ and $Z^o_{\rm dp}$ are simply propagated from errors in the reflectivity observations, as in the real data. Simulated observations of V^o_r and $K^o_{\rm DP}$ are obtained from the error-free V^t_r and $K^t_{\rm DP}$ by adding Gaussian errors of zero mean and specified SDs:

$$V^o_r = u\cos\alpha\sin\beta + v\cos\alpha\cos\beta + w\sin\alpha + \text{a random error} \quad \text{and} \tag{3}$$

$$K^o_{\rm DP} = K^t_{\rm DP} + \text{a random error.} \tag{4}$$

In (3), we neglected the effect of the hydrometeor terminal velocity, which is also done in this paper when assimilating V_r data. The same is done in XTD06, although our more recent studies have included the terminal velocity effect (TX08a).

We note that in (1)–(4) only the typical radar sampling error is simulated. Other types of measurement errors associated with mismatched side lobes, clutter contamination, partial beam filling, range effect, etc., are not taken into account in our error model. In our radar emulator, the SDs or variances can be specified by the user. For operational WSR-88D radars, the reasonable range of the standard deviations of reflectivity and differential reflectivity are 1–2 dBZ and 0.1–0.3 dB, respectively (Ryzhkov et al. 2005; Doviak and Zrnic 1993). The standard error of $K_{\rm DP}$ in the range of 0.24°–0.48° km^{-1} is expected for lightly filtered estimates of $K_{\rm DP}$ from differential phase $\phi_{\rm DP}$ for operational WSR-88Ds (Ryzhkov et al. 2005). The V_r error can be assumed to be 1 m s^{-1} (Doviak and Zrnic 1993).

Default error SDs used in our simulation and assimilation experiments are given here. The default values of $\varepsilon_{\rm corr}$ and ε_h (and ε_v) are set to be 36% and 2% of Z^t_h, so as to yield an effective error SD of about 2 dBZ for Z^o_H and close to 0.2 dB for $Z^o_{\rm DR}$. Gaussian errors with zero mean and SDs of 1 m s^{-1} for V^o_r and 0.5° km^{-1} for $K^o_{\rm DP}$, which is reasonable for a 2-km resolution (Ryzhkov et al. 2005), are added to V^t_r and $K^t_{\rm DP}$. The $(Z^o_{\rm dp})^{0.2}$ error is determined by the errors in Z^o_H, and is about 1.0 mm^6 m^{-3}. These errors approach the large end of errors suggested in the literature. Also, Torres and Zrnic (2003) proposed a technique that can significantly reduce statistical errors while maintaining the same level of current WSR-88D radar capabilities such as the scan rate. We assume large errors in the observations to account for the worst cases. The errors in the real observation can be reduced by implementing new techniques in the future, and then the impacts could be larger than those shown later in this paper. The same SDs (or their squared version, i.e., the error variances) are specified in the filter for the corresponding observations in all experiments presented in this paper.

As an example, Fig. 1 shows the error-containing (Figs. 1b,d,f) observations at the lowest radar elevation of 0.5° that are compared with the error-free observations (Figs. 1a,c,e), for the simulated supercell storm. Observations below 250 m in height, which is the first level of the scalar variables in the model for the 500-m vertical grid resolution, are not plotted near the radar at the lower-left-hand corner of each panel. With the default SD errors for Z_H, Z_V, $Z_{\rm DR}$, and $K_{\rm DP}$ as given above, the overall patterns of error-containing observations are not much affected by the errors. Of course, the error-containing observation fields appear noisy and the values at specific points differ from the truth values. Some local extrema introduced by the errors, like those at $x = 25$ and $y = 43$ km and at $x = 45$ and $y = 47$ km in the reflectivity field, are evident and resemble real observations (Fig. 1b). In our previous OSSE studies, negative Z_H is set to 0. This is done here also.

The errors in $Z_{\rm DR}$ are simply propagated from the errors in reflectivity at horizontal and vertical polarizations. Even though a large reflectivity error generally leads to a large $Z_{\rm DR}$ error in most cases, their errors are not necessarily strongly correlated at every point because of the uncorrelated part of error. The noise in the data is particularly noticeable for small values of $Z_{\rm DR}$ and most of this noise is removed in our assimilation by data thresholding. Negative $Z_{\rm DR}$ is also set to 0 as we assume that the differential attenuation is small for S-band radars at both polarizations, which could cause negative $Z_{\rm DR}$ by attenuating Z_H more than Z_V. Also, the negative $Z_{\rm DR}$ observed from hail (Bringi et al. 1986; Illingworth et al. 1987), either from prolate or conical shape particles or three-body scattering (Hubbert and Bringi 1997), is not simulated in this study; they are less important because they will most likely fall below our threshold. We also note here that setting the negative value to zero is also a form of data thresholding; we believe doing so is desirable and can be done with real data also.

We keep the negative values of $K_{\rm DP}$ in the error-containing field (Fig. 1f). An SD of 0.5° km^{-1} that is used here is quite large considering the dynamic range of data. However, the fact that $K_{\rm DP}$ error does not scale with the signal (as those of reflectivity do) means that the signal-to-noise ratio of $K_{\rm DP}$ is actually high in heavy precipitation regions.

b. Data assimilation procedure

As mentioned earlier, the EnKF radar data assimilation framework of XTD06, which was based on TX05

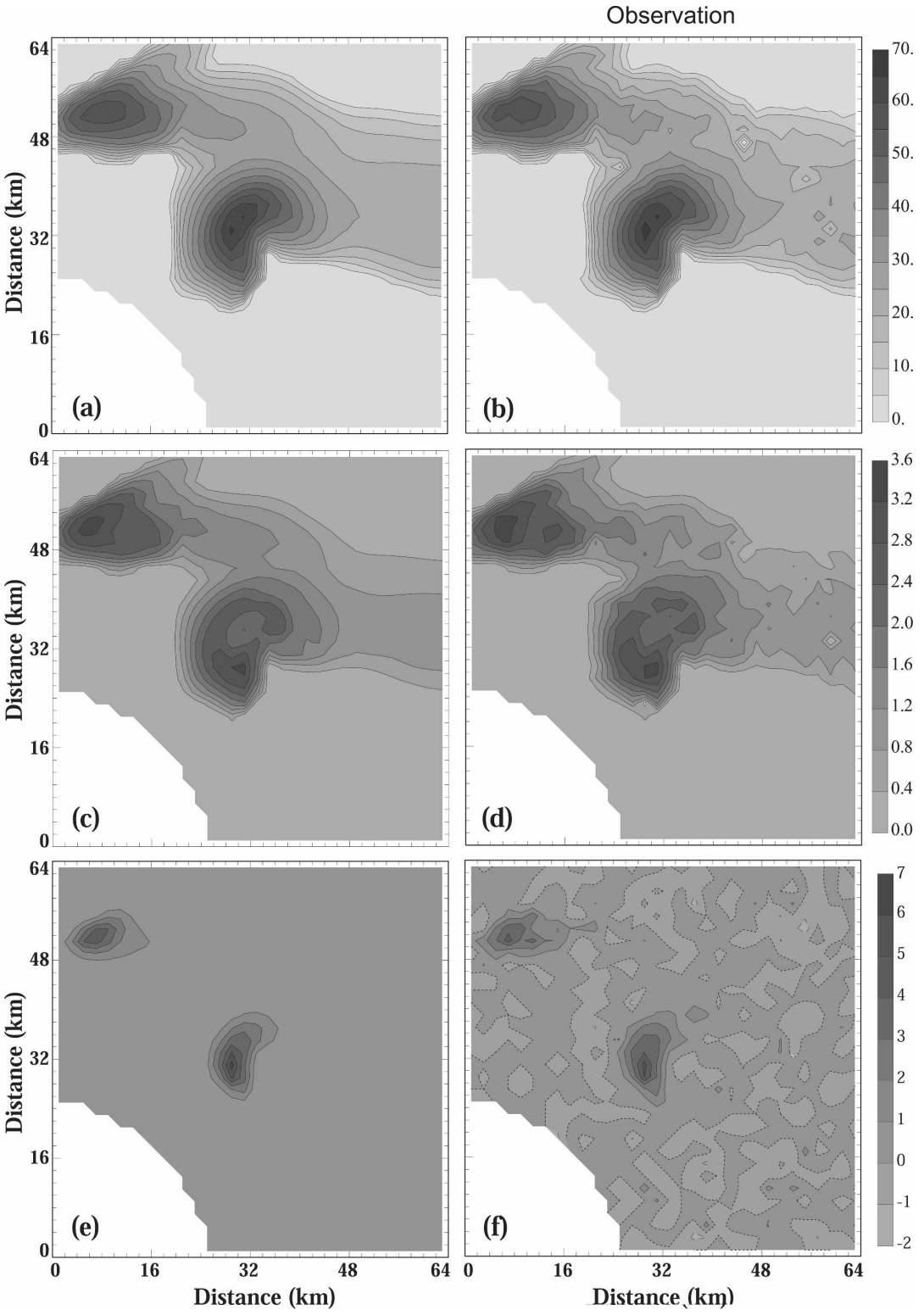

FIG. 1. Simulated (a),(c),(e) error-free and (b),(d),(f) error-containing observations at the 0.5° elevation at 100 min of the supercell storm simulation of (a),(b) Z_H; (c),(d) Z_{DR}; and (e),(f) K_{DP}.

and further enhanced in TX08a, is used as the basis of our data assimilation work. This framework is enhanced by adding additional capabilities to assimilate the polarimetric radar variables. The observation operators developed in Part I are used, with our formula for the reflectivity at horizontal polarization [(5) in Part I] replacing the reflectivity formula described in TX05. The new error model described above is used.

Our EnKF assimilation system employs the ensemble square-root filter (EnSRF) after Whitaker and Hamill (2002), which is a particular variant of ensemble-based filters. A full description of the filter can be found in XTD06 and TX08a. The experiment environment is largely inherited from XTD06 and TX08a, with the differences noted above.

Following TX08a, initial ensemble members are initialized at $t = 20$ min of model time by adding spatially smoothed perturbations to the initially horizontally homogeneous first guess defined by the Del City, Oklahoma, sounding. The standard deviations of the perturbations added to each variable are 2 m s^{-1} for u, v, and w; 2 K for θ; and 0.6 g kg^{-1} for the mixing ratios of hydrometeors (q_v, q_c, q_r, q_i, q_s, and q_h). The perturbations are added to the velocity components, potential temperature, and specific humidity, in the entire domain excluding grids composing the lateral boundaries. For the mixing ratios, the perturbations are added only to the grid points located within 6 km horizontally and 2 km vertically from the observed precipitation. Negative values of mixing ratios after the perturbations are added are reset to zero. The pressure variable is not perturbed. These configurations are the same as in TX08a.

The first assimilation of simulated observations is performed at 25 min of model time and the analyses are repeated every 5 min until 100 min. The filter uses 40 ensemble members and a covariance inflation factor of 15% and a covariance localization radius of 6 km (Anderson 2001; Xue et al. 2005; Houtekamer and Mitchell 1998, 2001; Hamill et al. 2001). A single virtual polarimetric WSR-88D radar that scans the model atmosphere is located at the southwest corner of the model domain, as is the nonpolarimetric radar in XTD06. For more detailed information on the configuration of the assimilation experiment, the reader is referred to XTD06 and TX08a.

c. Experimental design

To examine the impact of assimilating polarimetric variables (Z_{DR}, Z_{dp}, and K_{DP}), in addition to the reflectivity at horizontal polarization (Z_H, which is what conventional WSR-88D radars observe) or in addition to both Z_H and V_r, on the analysis of the convective storm, we designed 10 experiments, which are listed in Table 1. Experiment Zh serves as the control run for the first set of the data impact experiments that include itself, ZhZdr, ZhZdp, ZhKdp, and ZhZZK. Experiments ZhZdr, ZhZdp, and ZhKdp test the impact of Z_{DR}, Z_{dp}, and K_{DP} data individually when assimilated in addition to Z_H. Experiment ZhZZK tests the combined impact of all three variables (Z_{DR}, Z_{dp}, and K_{DP}) together. Experiment VrZh is the control run for the second set of experiments that consists of itself, VrZhZdr, VrZhZdp, VrZhKdp, and VrZhZZK. In this set, the impact of polarimetric variables in addition to both radial velocity and conventional reflectivity data is examined.

TABLE 1. List of experiments testing the impact of polarimetric variables.

Expt	Observation(s) assimilated
Zh	Z_H (everywhere)
ZhZdr	Z_H and Z_{DR} ($Z_{DR} > 0.3$ dB)
ZhZdp	Z_H and Z_{dp} [$(Z_{dp})^{0.2} > 1.7$ mm^6 m^{-3}]
ZhKdp	Z_H and K_{DP} ($K_{DP} > 0.9°$ km^{-1})
ZhZZK	Z_H, Z_{DR}, Z_{dp}, and K_{DP}
VrZh	V_r ($Z_H > 10$ dBZ) and Z_H
VrZhZdr	V_r, Z_H, and Z_{DR}
VrZhZdp	V_r, Z_H, and Z_{dp}
VrZhKdp	V_r, Z_H, and K_{DP}
VrZhZZK	V_r, Z_H, Z_{DR}, Z_{dp}, and K_{DP}

TX05 shows that the Z_H data from echo-free regions help suppress spurious cells in those areas. The Z_H data within the entire radar range are therefore assimilated in all of our experiments. For the polarimetric variables, thresholds that are experimentally determined are applied to each variable. We performed experiments ZhZdr, ZhZdp, and ZhKdp without thresholding and with various thresholds based on their SDs and found that applying thresholds can lead to better analyses. The thresholds used for Z_{DR}, $(Z_{dp})^{0.2}$, and K_{DP} in this study are 0.3 dB, 1.7 mm^6 m^{-3}, and 0.9° km^{-1}, respectively. In other words, we assimilate polarimetric variables only when their values are greater than their respective thresholds.

To help to understand the need for thresholding for polarimetric variables, we investigate the effect of observational errors on the analysis in the current assimilation framework. In our single-moment microphysics scheme, all polarimetric variables including Z_{DR} are uniquely determined by the mixing ratios only, with assumed fixed values of DSD parameters. Therefore, they are to some extent correlated with each other. In practice, assimilating two (or more) observations taken at the same point and time that should be correlated may result in the deterioration of the analysis if the

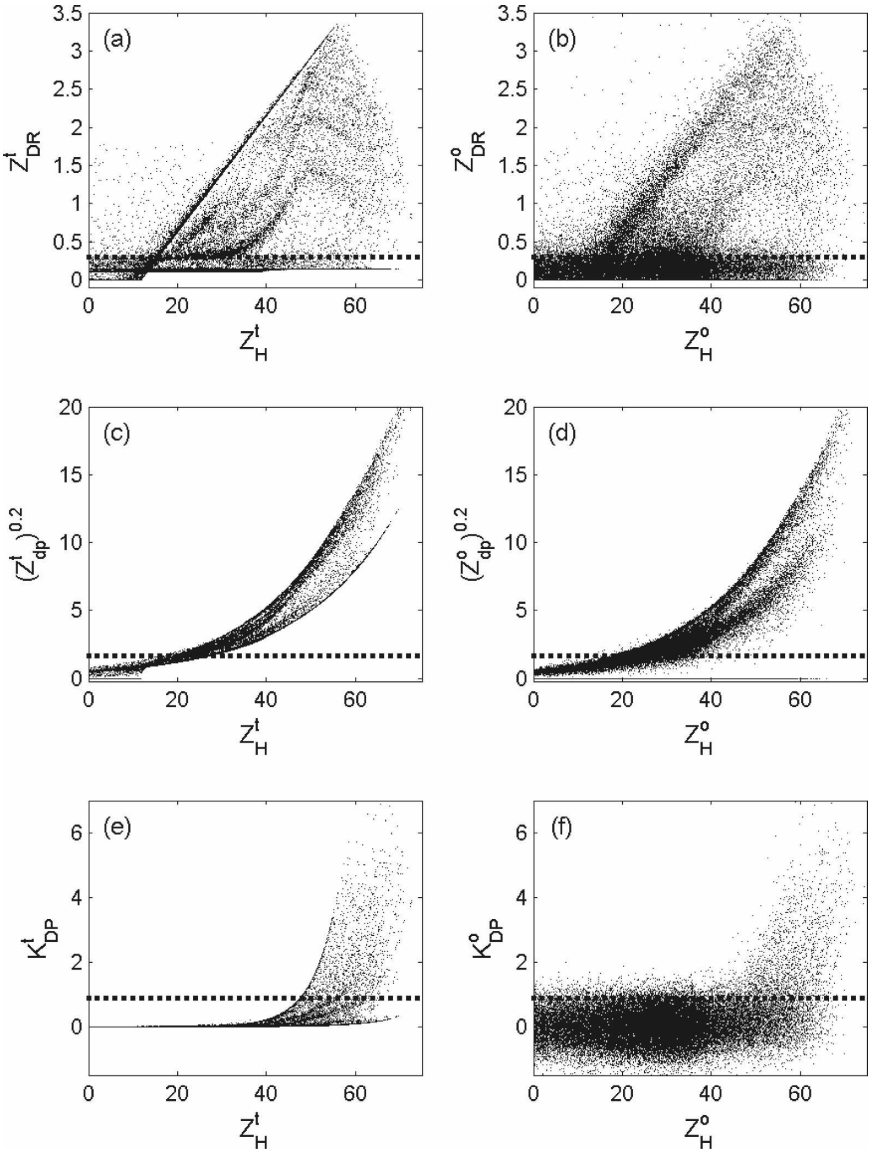

FIG. 2. Scatterplot of reflectivity vs (a),(b) differential reflectivity; (c),(d) reflectivity difference; and (e),(f) specific differential phase for (a),(c),(e) truth and (b),(d),(f) observation. The thresholds applied to the observation in the assimilation are overlaid on each plot (thick dashed).

noise level is high in one or both observations. When a signal is weak, as is often the case with polarimetric data in many parts of a storm (see examples given in Part I and here in Fig. 1), it is possible that the noise dominates over the signal. In such a case, the assimilation of noise-dominated data may interfere with the assimilation of signals contained in other variables that are less susceptible to the noise (e.g., reflectivity). This can be inferred from the scatterplots of polarimetric variables versus reflectivity in Fig. 2. Figures 2a,c,e show the scatter diagram between truth (error free) reflectivity and truth (error free) polarimetric variables and Figs. 2b,d,f show the same plots between error-containing observations. It is clear from the plots that the relative errors are larger for small values and smaller for large values. In Figs. 2a,e, there are several lines showing high population densities of observation points that pack together. When a single hydrometeor dominates in many of the radar sampling volumes, such as snow at the upper levels and rain at the low levels, the functional relation between the reflectivity and the polarimetric variable stands out as a densely clustered curve. In Fig. 2a, the straight steeply sloped line corresponds to raindrops. In the error-free cases, all scatter

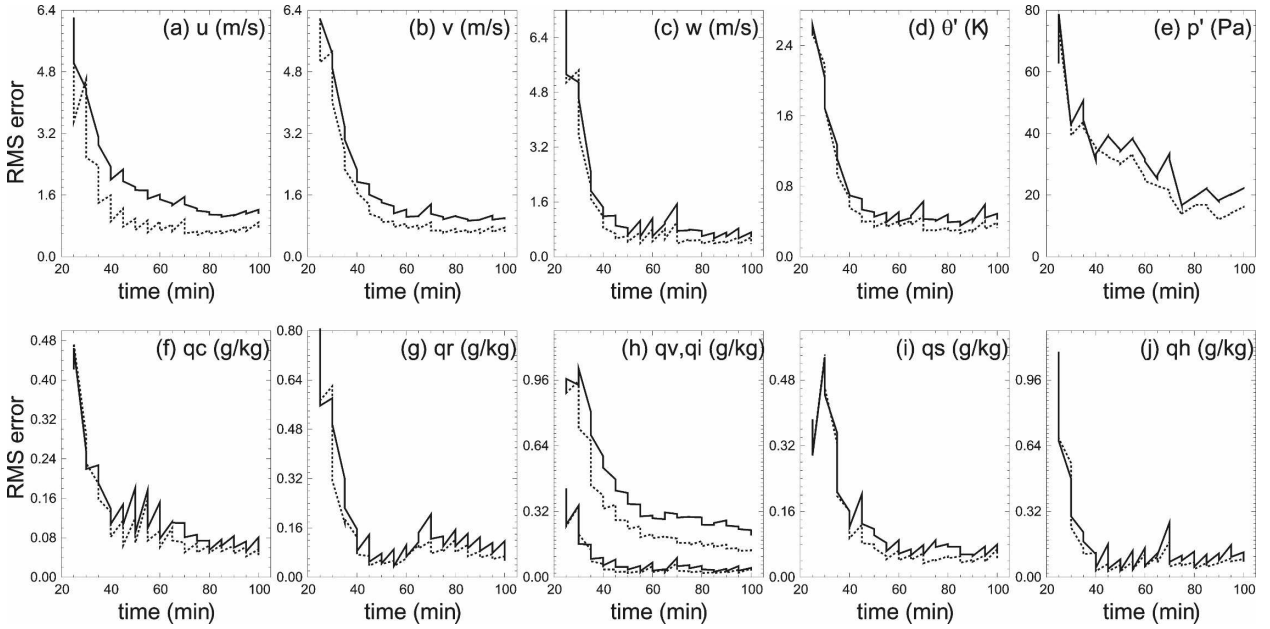

FIG. 3. The ensemble mean forecast and analysis RMSEs averaged over points at which the true reflectivity is greater than 10 dBZ for (a) u, (b) v, (c) w, (d) perturbation potential temperature θ', (e) p', (f) q_c, (g) q_r, (h) q_v (the curves with larger values) and q_i (the curves with lower values), (i) q_s, and (j) q_h for experiments Zh (solid black) and VrZh (dotted black). The vertical straightline segments in the curves correspond to the reduction or increase in RMSEs or ensemble spreads by the data assimilation.

away from the identifiable curves is due to the coexistence of more than one hydrometeor species in the sampling volumes. For those who are interested in more detailed information on the impacts of noise on signals, many past studies are well documented in Doviak and Zrnic (1993) and Bringi and Chandrasekar (2001).

When the simulated errors are added to the error-free observations, the clearly defined lines become blurred, and overall there is much more scatter within the plots (Figs. 2b,d,f). For reflectivity difference $(Z_{\rm dp})^{0.2}$ (Figs. 2c,d), the line broadening due to noise is more severe where the slope is low below a certain threshold. As a result, the reflectivity shows a much larger variability for small values of $(Z_{\rm dp})^{0.2}$ in Fig. 2d. For $K_{\rm DP}$, the effect of noise at low $K_{\rm DP}$ values is even more severe—below $K_{\rm DP} = 0.9$, no signal is perceivable due to noise (Fig. 2f). For this reason, the thresholding of polarimetric variables is clearly necessary, and their values are chosen based on the scatterplots in combination with sensitivity experiments, at levels below which noise dominates, as indicated by the horizontal dashed lines in the plots. These thresholds are applied to the simulated data. When the thresholds are increased above these levels, we found that the quality of analysis starts to decline because some useful signal is excluded. With the given thresholds, only 34.5%, 53.6%, and 13.9% of $Z_{\rm DR}$, $Z_{\rm dp}$, and $K_{\rm DP}$ observations, respectively, collected from the echo region (where observed reflectivity is greater than 0 dBZ) are assimilated. If more data could be used, the impact of polarimetric data to be shown later might have been larger.

3. The impact of assimilating polarimetric variables

We examine, through the two sets of experiments listed in Table 1, the impact of $Z_{\rm DR}$, $Z_{\rm dp}$, and $K_{\rm DP}$ data when only Z_H is assimilated or when both V_r and Z_H are assimilated. The V_r data are only available in precipitation regions where reflectivity is greater than 10 dBZ following TX05.

Figure 3 shows the ensemble mean analysis and forecast RMSEs of model state variables during the assimilation cycles of experiments Zh and VrZh, which are our control runs. As in TX05 and XTD06, these errors are calculated in the regions where the truth reflectivity (Z_H^t) is no less than 10 dBZ. Additional details on the plots can be found in those papers. As mentioned earlier, the experiment names are self-descriptive. For example, experiment Zh assimilates Z_H data only and ZhZdr assimilates Z_H and $Z_{\rm DR}$ while experiment VrZhZZK assimilates V_r, Z_H, $Z_{\rm DR}$, $Z_{\rm dp}$, and $K_{\rm DP}$.

Under the perfect model assumption, the solid curves in Fig. 3 show that reflectivity data alone can successfully reduce the RMSEs over the first 40 min or so of

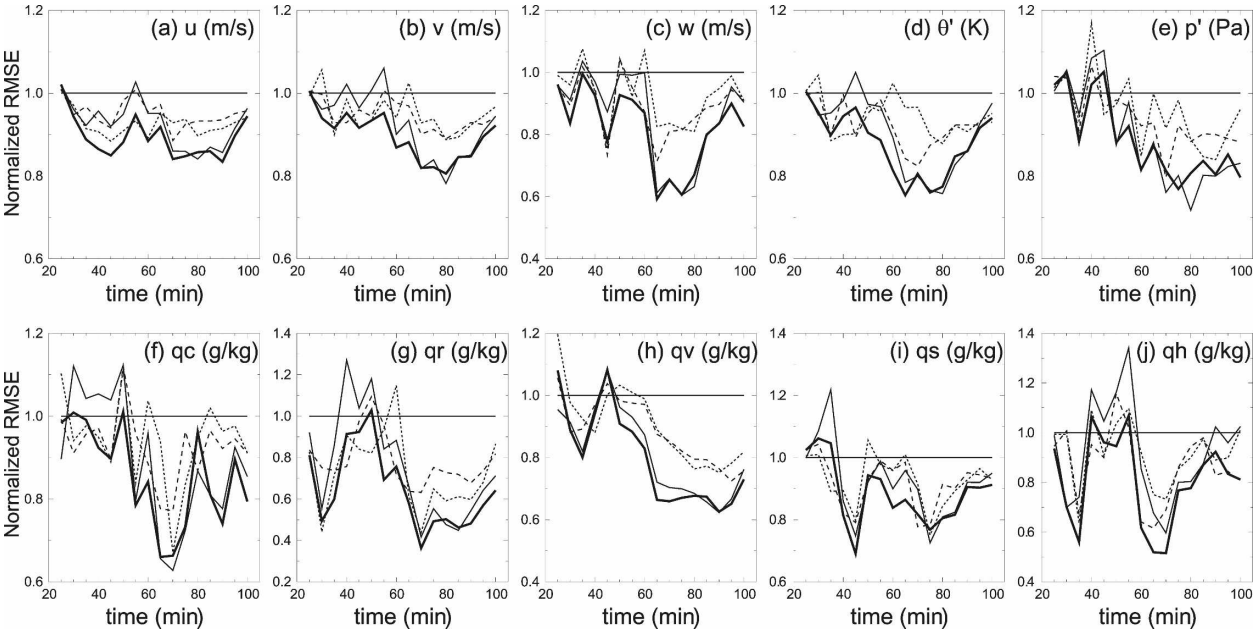

FIG. 4. The ensemble mean analysis RMSEs of experiments ZhZZK (thick solid), ZhZdr (solid), ZhZdp (dashed), and ZhKdp (dotted) normalized by those of experiment Zh. The reference horizontal line at unity is overlaid.

the assimilation window period to rather low levels. After $t = 60$ min, the RMSEs more or less stabilize. At the end of the assimilation window, the RMSEs of u and v are between 1 and 1.2 m s^{-1}, while that of w is about 0.6 m s^{-1}. The RMSEs of the hydrometeors are all below 0.1 g kg^{-1} except for q_v. On average over all assimilation cycles, an additional 30%–48% of analysis error reduction in u, v, and w, and 17%–27% in the rest of the variables except for q_v, which shows about 36% of error reduction, are achieved with the addition of V_r data. These results are consistent with those of TX05.

Because we are interested in if and how much the polarimetric data can further improve the analyses when they are assimilated in addition to reflectivity or both reflectivity and radial velocity data, we normalize the ensemble mean analysis RMSE of the data impact experiments using those of the corresponding control. Namely, the RMSEs of ZhZdr, ZhZdp, ZhKdp, and ZhZZK are normalized by the errors of Zh, and the errors of VrZh are used to normalize those of VrZhZdr, VrZhZdp, VrZhKdp, and VrZhZZK. [These normalized RMSEs (NRMSEs) are shown in Figs. 4 and 6]. A smaller NRMSE suggests a larger improvement through the assimilation of additional variable(s).

Figure 4 shows that every polarimetric variable shows a degree of positive impact when assimilated individually in addition to reflectivity (Fig. 4), at least during the later assimilation cycles when the filter stabilizes. Generally, ZhZdp (dashed in Fig. 4) and ZhKdp (dotted in Fig. 4) produce better analyses than ZhZdr (solid in Fig. 4) during early-to-intermediate cycles and ZhZdr shows a bigger improvement than ZhZdp and ZhKdp during intermediate-to-later cycles. These results show that different observations may have different relative impact at the different times. At the early stage of assimilation when the forecast error is relatively large, the intensity information carried by Z_{dp} and K_{DP} seems to be more beneficial. Later in the assimilation period, Z_{DR} seems to provide additional information other than intensity.

From experiments ZhZdp, ZhZdr, and ZhKdp, with the help of any one of the polarimetric variables, the normalized analysis RMSEs stay lower than those of experiment Zh after 60 min of model time for all variables except for q_h, but there is a tendency for such error reductions to become smaller in the later assimilation cycles for many of the variables. This is believed to be due to the fact that by the time of the later cycles, the reflectivity data have had more time to correct the model state error while during the intermediate cycles, there is more room for the polarimetric variables to contribute, by accelerating the error reduction. During the earlier cycles, the positive impact of the polarimetric variables is questionable according to Fig. 4, which suggests that when the model state estimation is relatively poor (during the earlier cycles), the positive impact of the polarimetric variables is harder to realize.

After 60 min of model time, in general, ZhKdp shows

the smallest error reduction among ZhZdr, ZhZdp, and ZhKdp on average. Their error reduction behaviors are all similar to each other with the exception of q_c and p' during the later assimilation cycles. Experiment ZhZdp shows generally larger RMSEs than ZhZdr, but slightly smaller than or similar to ZhKdp in most variables. The polarimetric variables are more beneficial to w, q_v, and q_r, with the reduction of error in q_r being the largest. This is probably not surprising because rainwater mixing ratio, q_r, is directly involved in the calculation of Z_{DR}, Z_{dp}, and K_{DP}, and the signatures of these variables are strongest where rain mixing ratio is larger (see Part I). These variables are related to w and q_v through their direct connection to the updraft/downdraft intensities and microphysics. For example, q_v converts to q_r through condensation in the updraft and is created from q_r by evaporation in the downdraft. Among the other state variables, the improvements to u, v, and q_s are rather smaller. Even though q_s is directly related to polarimetric variables, the polarimetric signatures related to dry-ice-phase hydrometeors are generally weak so that most of the observations containing information on q_s are screened out by the observation thresholding. An interesting point is that the analysis error reduction is relatively large in q_h. This is because a considerable amount of q_h information is available from wet hail, which survives the thresholding in the deep layer below the melting level.

Among experiments ZhZdp, ZhZdr, and ZhKdp, experiment ZhZdr has the greatest impact. This may not be intuitively obvious because Z_{DR} mainly carries information on the difference between reflectivity at the horizontal and vertical polarization; however, it does not provide much information on the intensity of the reflectivity. On the contrary, K_{DP} and Z_{dp} are directly related to mixing ratios and are expected to be more useful for quantification. This behavior may be explained in terms of independent information content. The Z_{DR} contains information on the mean shape and orientation of hydrometeors and is proportional to the median diameter of precipitation particles in the radar resolution volume. The Z_H is mainly related to the hydrometeor concentration. For rain drops, the shape is a strong function of size and, therefore, Z_{DR} and Z_H share some information in common. Both K_{DP} and Z_{dp} contain the information on both hydrometeor concentration and shape. As discussed earlier in section 2c, with a single-moment scheme, all polarimetric variables are correlated to the reflectivity, with the correlation between Z_{DR} and Z_H being the smallest; the independent information content in Z_{DR} can therefore have a larger impact. The intensity information should have already been well captured by the Z_H data. Another perhaps more important issue is that, with the current single-moment microphysics scheme used, the DSD parameters, including intercept parameters and hydrometeor densities, are fixed and cannot be adjusted using the information contained in the polarimetric radar data. The impact of polarimetric data may increase when adjustments to these parameters are allowed, via, for example, parameter estimation (TX08a and TX08b) or if a multimoment scheme is used. In those cases, the response of the data assimilation system to the polarimetric data may become more physical.

When all three polarimetric variables are assimilated together, the analysis improvement is seen to further increase in general, although ZhZdr does do better temporarily after 60 min of model time for p', ZhZdp does better for q_r and q_h, and ZhKdp does better for p'. It is encouraging that experiment ZhZZK successfully reduces the analysis RMSEs even when individual polarimetric parameters show little or no positive impact. For instance, the normalized RMSEs of ZhZZK stay low at 65 min of model time for q_s, at 85 min for q_c, and at 90 and 100 min for q_h, while the corresponding RMSEs of ZhKdp, ZhZdr are greater than 1.

From Fig. 4j, we see that K_{DP} and Z_{dp} help reduce the RMSE up to 60 min, Z_{DR} helps reduce the RMSE from 60 to 85 min, and Z_{dp} helps reduce the RMSE after 85 min. Similar behaviors are seen in many other variables (Figs. 4a–c,f,g).

The percentage improvement over experiment Zh averaged over the last nine cycles is summarized in Table 2. From Table 2, we can see that all model state variables experience analysis error reduction when assimilating polarimetric data. The improvement is greatest in q_r, which has an approximately 29%–41% improvement in ZhZdr, ZhZdp, and ZhKdp and more than 50% improvement when all three variables are assimilated. As discussed in the Part I, K_{DP} is more linearly proportional to rain mixing ratio and has little sensitivity to other species. Therefore, it is expected to be more useful for determining q_r than other variables, including Z_H, even if we take the thresholding into account. Actually, only 14% of available K_{DP} observations are used in the analysis, which is about 40% of Z_{DR} and about 25% of Z_{dp} observations. Considering this, the impact of K_{DP} on q_r analysis is rather large.

Figure 5 shows the vertical profiles of the RMSEs averaged over points at which the truth reflectivity is greater than 10 dBZ for experiments Zh (dotted) and ZhZdr (solid) at 80 min. It is seen that the errors of all variables are reduced at almost all levels by assimilating Z_{DR}, with the exceptions being with u in a shallow layer between 12.5- and 13.0-km height. Considering that

TABLE 2. The improvement over the experiment Zh for the experiments ZhZdr, ZhZdp, ZhKdp, and ZhZZK and over the experiment VrZh for the experiments VrZhZdr, VrZhZdp, VrZhKdp, and VrZhZZK averaged over the last nine cycles (60–100 min of model time). The improvement is expressed in percentages relative to the corresponding control experiment.

	Improvement (%)				Improvement (%)			
Variable	ZhZdr	ZhZdp	ZhKdp	ZhZZK	VrZhZdr	VrZhZdp	VrZhKdp	VrZhZZK
u	10.4	6.2	7.8	14.6	5.0	2.8	4.4	7.1
v	13.1	7.2	6.1	17.1	0.7	0.8	3.0	1.2
w	22.3	14.4	9.7	28.3	12.3	7.3	7.1	18.7
θ'	15.7	10.6	6.2	19.6	3.2	2.6	4.6	7.4
p'	19.7	10.8	9.1	20.0	8.6	2.0	4.9	11.9
q_v	29.0	18.3	17.5	33.5	9.5	5.1	3.9	9.9
q_c	20.0	11.0	7.8	23.4	8.1	5.2	4.7	12.9
q_r	40.7	28.7	31.1	51.9	31.1	22.1	30.5	45.9
q_i	15.0	8.4	9.4	21.9	4.0	4.2	7.8	9.3
q_s	12.2	9.5	9.0	18.4	3.0	2.2	1.1	6.7
q_h	15.4	19.9	11.8	26.1	3.2	8.8	7.2	14.4
Tot	213.5	145.0	125.5	274.8	88.7	63.1	79.2	145.4

most Z_{DR} observations at the high altitudes are excluded by the threshold constraints (see Table 1) because Z_{DR} values are typically small for ice phase particles (see Fig. 6 of Part I), the fact that improvements are found at all levels is encouraging specially with the large error reduction at the upper levels in v, w, θ', and q_s. Also, the error reduction is generally largest where the RMSE profiles peak. Apparently, direct improvement to the analysis at the low levels is propagated upward, or throughout the computational domain, through the dynamic prediction model. The reduction of errors in q_r and q_h below 5 km where the melting occurs is also noticeable at the time shown.

In the next set of experiments (VrZh, VrZhZdr, VrZhKdp, and VrZhZZK), we examine the impact of Z_{DR}, Z_{dp}, and K_{DP} data when both V_r and Z_H are assimilated. From Fig. 6, we see that in such a case, the impact of polarimetric variables is rather small though still positive in general during middle to later cycles in most of the state variables although temporary deterioration can occur with q_s and q_h. Variables u and w show decreasing error reduction starting around 80 min of model time and the RMSE reduction is minimized at the end of assimilation cycles while the improvement is very small in v. Such a diminishing impact of the additional polarimetric variables appears again due to the

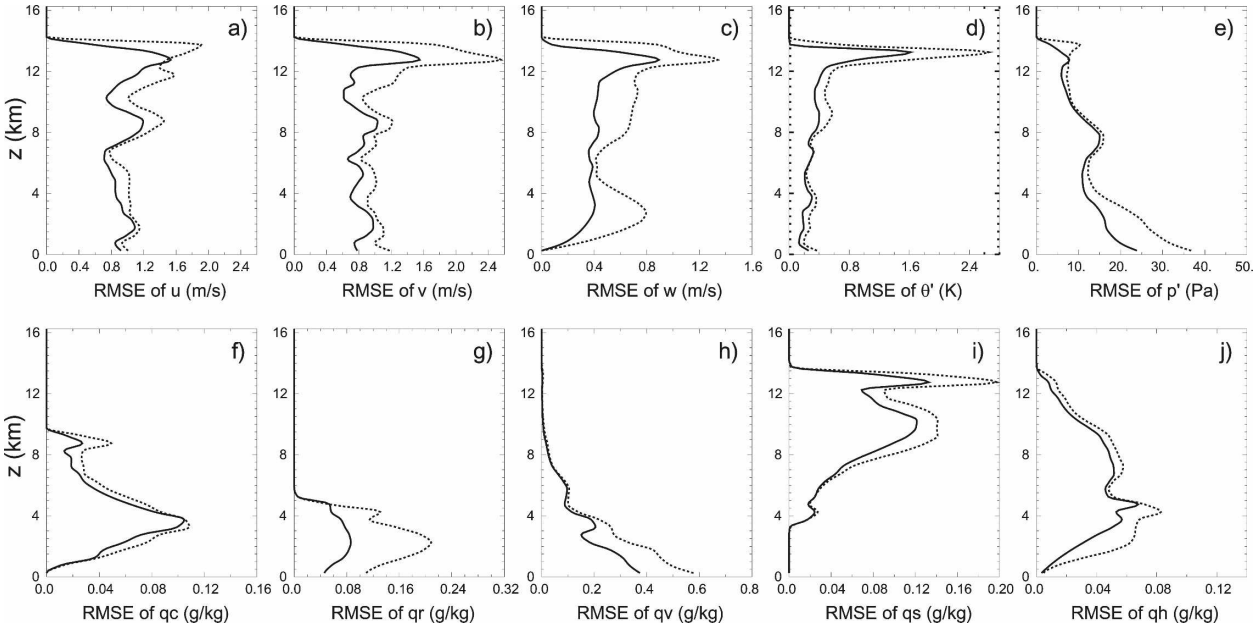

FIG. 5. The vertical profile of RMS analysis errors averaged over points at which the truth reflectivity is greater than 10 dBZ for (a) u, (b) v, (c) w, (d) θ', (e) p', (f) q_c, (g) q_r, (h) q_v, (i) q_s, and (j) q_h at 80 min of experiments Zh (dashed) and ZhZdr (solid).

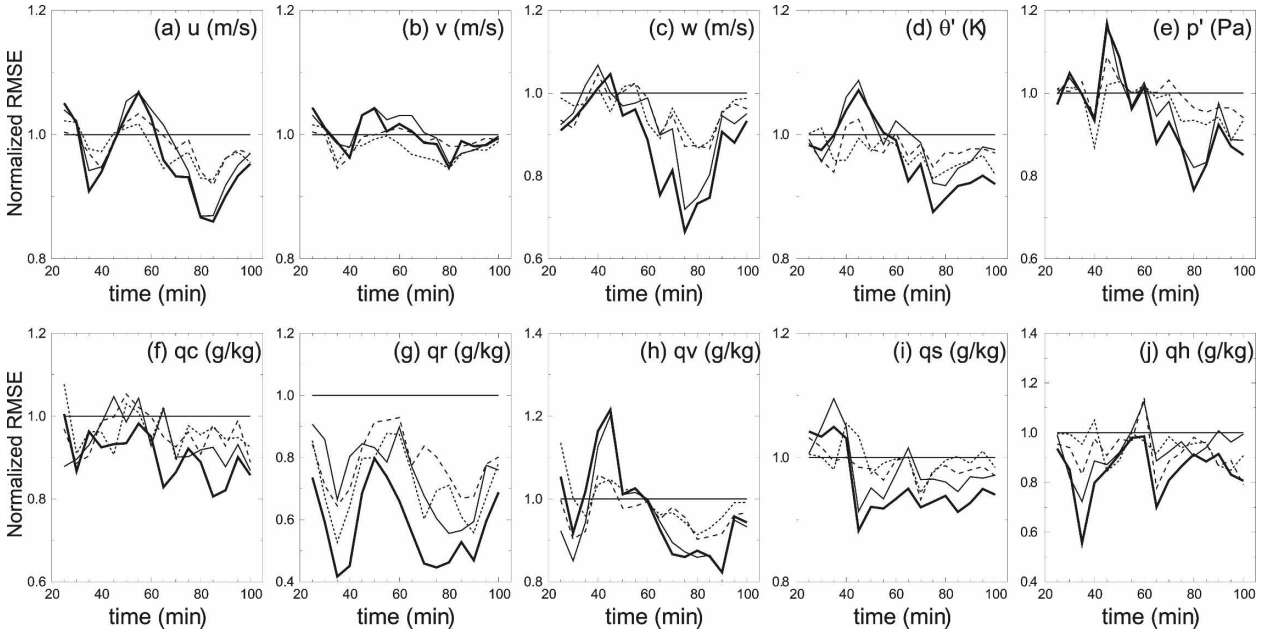

FIG. 6. As in Fig. 4, but for experiments VrZhZZK (thick solid), VrZhZdr (solid), VrZhZdp (dashed), and VrZhKdp (dotted).

very accurate analysis that one can already achieve by using reflectivity and radial velocity data, especially after they have had a sufficiently long time to contribute to the state estimation.

The gross improvement can be assessed more easily from Table 2. The error reduction characteristics are generally similar to but somewhat different from those of the previous set of experiments. As in previous cases, the improvement is generally larger in w, q_v, and q_r and smaller in u, v, and q_s either when polarimetric variables are assimilated individually or when all are assimilated together. Again, q_h shows large improvement, even larger than those of w and q_v in VrZhZdp and VrZhKdp, and than that of q_v in VrZhZZK. Another interesting point is that the gross error reduction by VrZhZdp is smaller than that of VrZhKdp, in contrast to the experiments without V_r. When V_r is assimilated, the percentage improvements by polarimetric variables relative to the control experiment are significantly reduced with the percentage reduction by K_{DP} being the smallest in general compared to the corresponding experiments without V_r. Moreover, the percentage improvement in q_r is similar between VrZhKdP and ZhKdp.

From Table 2, we can see that the NRMSE reduction by VrZhh for the 11 model state variables range from 1% to 46% when all polarimetric data are assimilated together. However, these additional error reductions may not be very meaningful in practice. Within the current OSSE framework using a perfect prediction model, the analysis obtained using V_r and Z_H alone is already very good; the RMS analysis errors in u and v, for example, are quickly reduced to below 1 m s^{-1} within 4–5 cycles (Figs. 3a–c), therefore there is little room for further improvement (the 1 m s^{-1} analysis error is already at or below the level of V_r RMSE, which is 1 m s^{-1} as defined in section 2). For real data cases where model error tends to be rather large, the extra information content afforded by the polarimetric data may produce a larger impact, especially when the polarimetric data are used to correct microphysics-related model error. For the single-moment scheme used here, many uncertainties exist with the values of the intercept parameters associated with the assumed exponential DSDs, and with snow and hail densities. TX08a shows that large analysis error can result when errors exist in these DSD parameters and the resultant analysis errors tend to be larger than the amount of error reduction achieved here through the assimilation of additional polarimetric variables. TX08a also shows that the errors in the DSD parameters can often be corrected through EnKF-based parameter estimation, although nonuniqueness in the solution does seem to exist. The final parameter estimation was found to be sensitive to the initial guess when multiple parameters are estimated together. It was suggested there that additional polarimetric data could impose additional constraints that may improve the uniqueness of the solution, given the fact that the polarimetric data contain DSD information. Using additional polarimetric pa-

rameters to improve the DSD parameter retrieval whereby reducing microphysical uncertainties and model error is the goal of our planned research, and is, we believe, where polarimetric data assimilation may play an even greater role.

Last, we also performed additional experiments assimilating combinations of any two of Z_{DR}, Z_{dp}, and K_{DP}, and these experiments exhibit lower analysis errors for most variables than experiments assimilating any one of the two variables involved in terms of time-averaged RMSEs after 60 min. One exception is found in q_h of ZhZdrZdp, whose time-averaged RMSE is smaller than that of ZhZZK. For example, ZhZdrKdp and ZhZdpKdp result in better analyses than those of ZhZdr and ZhKdp in terms of RMSE, but worse analyses than that of ZhZZK. This is also true when V_r is assimilated. In this case, VrZhZZK produces the best analyses among all experiments including those assimilating any two combinations of polarimetric variables with one exception in v of VrZhZdpKdp. So in general, it is better to assimilate more polarimetric variables.

4. Summary and further discussion

In this paper, an ensemble Kalman filter system that incorporates the ability to assimilate polarimetric radar variables is described. It employs the observation operators developed in the first part of this paper. The polarimetric variables considered include the differential reflectivity Z_{DR}, reflectivity difference Z_{dp}, and specific differential phase K_{DP}. A new error model for reflectivities at horizontal and vertical polarizations is developed in this study that includes both correlated and uncorrelated errors, and the relative errors of which are assumed to have Gaussian distributions in the linear domain based on Xue et al. (2007). This model gives realistic errors for the derived quantities, such as Z_{DR} and Z_{dp}. The simulated error-containing radar observations are shown, for example, for the truth simulation of a supercell.

The enhanced EnKF assimilation system is used to assimilate radar data sampled from a simulated supercell storm, to examine the impact of additional polarimetric measurements, including Z_{DR}, Z_{dp}, and K_{DP}, on the quality of storm analysis under the perfect model assumption. It is found that the assimilation of these variables, in addition to the reflectivity at horizontal polarization (reflectivity measurement of nonpolarimetric radars), helps further reduce the analysis error and the improvement during the intermediate and later assimilation cycles can be quite significant for some state variables. The results also show that the analyses for all model state variables are improved at all vertical levels in general. Although Z_{DR} does not directly reflect the magnitude of hydrometeor concentration, it gives the largest impact among the three polarimetric variables examined. When both V_r and Z_H are assimilated, the impact of additional polarimetric variables becomes smaller, partly because the analyses obtained with V_r and Z_H alone are already very good.

The results show that applying data thresholding when assimilating polarimetric variables leads to better analysis. When two or more observations are taken at the same point and time that are somewhat correlated, the assimilation of noise-containing observations may interfere with the assimilation of signals contained in other observations. This noise effect can limit the improvement to the analysis or even harm the analysis, especially when the noise level is high, which is likely to be true where a signal is weak. Applying thresholding also reduces the assimilation cost.

It is suggested that polarimetric radar data can be very useful for estimating DSD parameters, such as the intercept parameters and hydrometeor densities used in single-moment microphysics schemes, because of their information content on DSDs. The DSD parameter estimation experiments using our EnKF framework are under way, following the work of TX08a and TX08b.

We expect to see a larger impact when a two-moment microphysics scheme is used and/or for real data cases where the state estimation using V_r and Z_H is generally not as good. When a two-moment scheme is used, Z_{DR} depends only on the slope parameter Λ, which is a function of mixing ratios, while Z_H depends on both total number concentration N_t and slope parameter Λ of the exponential and the gamma DSD. In that case, Z_{DR} is expected to be more independent of Z_H. Even though K_{DP} and Z_{DP} are still correlated with Z_H as they are determined by N_t and Λ, as is Z_H, a two-moment scheme will increase the number of model state variables to be estimated, and then V_r and Z_H data alone may become insufficient to estimate all state variables. In such cases, additional polarimetric data are expected to play a larger role.

We also pointed out earlier that the error levels assumed for the polarimetric variables are on the larger side. The data thresholding necessitated by the relatively larger errors caused the discarding of large fractions of the simulated polarimetric observations. If the actual errors are smaller, larger impacts may be expected.

Last, we point out that even though correlations among the reflectivity-related observation variables and their errors are expected, in the EnSRF used here, which assimilates observations serially, one at a time, all observations are assumed to be uncorrelated. The

ideal way of processing correlated observations is to either transform the observation variables into a space where the assimilated quantities are no longer correlated (this may or may not be possible) or to use an algorithm that can take the observation error covariance into account. Their practical implementations are often nontrivial, however. To have an idea how much our observation errors are correlated, we calculated the observational error correlation coefficients between Z_H and the polarimetric variables and found the coefficients to be 3.8×10^{-2}, 0.37, and -3.2×10^{-3} for those between Z_H and Z_{DR}, $(Z_{\mathrm{dp}})^{0.2}$, and K_{DP}, respectively. These correlations suggest that the results of our serial algorithm are probably reasonable.

Acknowledgments. The authors thank Mingjing Tong for her help on the initial use of the ARPS ensemble Kalman filter code. This work was primarily supported by NSF Grants EEC-0313747 and ATM-0608168. Ming Xue was also supported by NSF Grants ATM-0530814, ATM-0331594, and ATM-0331756 and by Chinese Natural Science Foundation Grant 40620120437, and Jerry Straka was supported by Grant ATM-0340639. The computations were performed at the Pittsburgh Supercomputing Center supported by NSF and at the OU Supercomputing Center for Education and Research. The suggestions and comments of the anonymous reviewers improved this paper.

REFERENCES

Anderson, J. L., 2001: An ensemble adjustment Kalman filter for data assimilation. *Mon. Wea. Rev.,* **129,** 2884–2903.

Bishop, C. H., B. J. Etherton, and S. J. Majumdar, 2001: Adaptive sampling with the ensemble transform Kalman filter. Part I: Theoretical aspects. *Mon. Wea. Rev.,* **129,** 420–436.

Bringi, V. N., and V. Chandrasekar, 2001: *Polarimetric Doppler Weather Radar*: *Principles and Applications*. Cambridge University Press, 662 pp.

——, J. Vivekanandan, and J. D. Tuttle, 1986: Multiparameter radar measurements in Colorado convective storms. Part II: Hail detection studies. *J. Atmos. Sci.,* **43,** 2564–2577.

Burgers, G., P. J. van Leeuwen, and G. Evensen, 1998: Analysis scheme in the ensemble Kalman filter. *Mon. Wea. Rev.,* **126,** 1719–1724.

Courtier, P., and O. Talagrand, 1987: Variational assimilation of meteorological observations with the adjoint equation. Part II: Numerical results. *Quart. J. Roy. Meteor. Soc.,* **113,** 1329–1347.

Doviak, R., and D. Zrnic, 1993: *Doppler Radar and Weather Observations*. 2nd ed. Academic Press, 562 pp.

Evensen, G., 1994: Sequential data assimilation with a nonlinear quasi-geostrophic model using Monte Carlo methods to forecast error statistics. *J. Geophys. Res.,* **99** (C5), 10 143–10 162.

——, 2003: The ensemble Kalman filter: Theoretical formulation and practical implementation. *Ocean Dyn.,* **53,** 343–367.

——, and P. J. van Leeuwen, 1996: Assimilation of *Geosat* altimeter data for the Agulhas Current using the ensemble Kalman filter with a quasigeostrophic model. *Mon. Wea. Rev.,* **124,** 85–96.

Hamill, T. M., J. S. Whitaker, and C. Snyder, 2001: Distance-dependent filtering of background error covariance estimates in an ensemble Kalman filter. *Mon. Wea. Rev.,* **129,** 2776–2790.

Houtekamer, P. L., and H. L. Mitchell, 1998: Data assimilation using an ensemble Kalman filter technique. *Mon. Wea. Rev.,* **126,** 796–811.

——, and ——, 2001: A sequential ensemble Kalman filter for atmospheric data assimilation. *Mon. Wea. Rev.,* **129,** 123–137.

——, ——, G. Pellerin, M. Buehner, M. Charron, L. Spacek, and B. Hansen, 2005: Atmospheric data assimilation with an ensemble Kalman filter: Results with real observations. *Mon. Wea. Rev.,* **133,** 604–620.

Hubbert, J. V., and V. N. Bringi, 1997: The effects of 3-body scattering on differential reflectivity. Preprints, *28th Conf. on Radar Meteorology,* Austin, TX, Amer. Meteor. Soc., 11–12.

Illingworth, A. J., J. W. F. Goddard, and S. M. Cherry, 1987: Polarization radar studies of precipitation development in convective storms. *Quart. J. Roy. Meteor. Soc.,* **113,** 469–489.

Jung, Y., G. Zhang, and M. Xue, 2008: Assimilation of simulated polarimetric radar data for a convective storm using the ensemble Kalman filter. Part I: Observation operators for reflectivity and polarimetric variables. *Mon. Wea. Rev.,* **136,** 2228–2245.

Le Dimet, F. X., and O. Talagrand, 1986: Variational algorithms for analysis and assimilation of meteorological observations: Theoretical aspects. *Tellus,* **38A,** 97–110.

Milbrandt, J. A., and M. K. Yau, 2005: A multimoment bulk microphysics parameterization. Part II: A proposed three-moment closure and scheme description. *J. Atmos. Sci.,* **62,** 3065–3081.

Ryzhkov, A. V., D. S. Zrnic, and B. A. Gordon, 1998: Polarimetric method for ice water content determination. *J. Appl. Meteor.,* **37,** 125–134.

——, S. E. Giangrande, V. M. Melnikov, and T. J. Schuur, 2005: Calibration issues of dual-polarization radar measurements. *J. Atmos. Oceanic Technol.,* **22,** 1138–1155.

Seliga, T. A., and V. N. Bringi, 1976: Potential use of radar differential reflectivity measurements at orthogonal polarizations for measuring precipitation. *J. Appl. Meteor.,* **15,** 59–76.

Snyder, C., and F. Zhang, 2003: Assimilation of simulated Doppler radar observations with an ensemble Kalman filter. *Mon. Wea. Rev.,* **131,** 1663–1677.

Straka, J. M., D. S. Zrnic, and A. V. Ryzhkov, 2000: Bulk hydrometeor classification and quantification using polarimetric radar data: Synthesis of relations. *J. Appl. Meteor.,* **39,** 1341–1372.

Tippett, M. K., J. L. Anderson, C. H. Bishop, T. M. Hamill, and J. S. Whitaker, 2003: Ensemble square-root filters. *Mon. Wea. Rev.,* **131,** 1485–1490.

Tong, M., and M. Xue, 2005: Ensemble Kalman filter assimilation of Doppler radar data with a compressible nonhydrostatic model: OSS experiments. *Mon. Wea. Rev.,* **133,** 1789–1807.

——, and ——, 2008a: Simultaneous estimation of microphysical parameters and atmospheric state with simulated radar data and ensemble square-root Kalman filter. Part I: Sensitivity analysis and parameter identifiability. *Mon. Wea. Rev.,* **136,** 1630–1648.

——, and ——, 2008b: Simultaneous estimation of microphysical

parameters and atmospheric state with simulated radar data and ensemble square-root Kalman filter. Part II: Parameter estimation experiments. *Mon. Wea. Rev.,* **136,** 1649–1668.

Torres, S. M., and D. S. Zrnic, 2003: Whitening in range to improve weather radar spectral moment estimates. Part I: Formulation and simulation. *J. Atmos. Oceanic Technol.,* **20,** 1433–1448.

Vivekanandan, J., V. N. Bringi, M. Hagen, and G. Zhang, 1994: Polarimetric radar studies of atmospheric ice particles. *IEEE Trans. Geosci. Remote Sens.,* **32,** 1–10.

Whitaker, J. S., and T. M. Hamill, 2002: Ensemble data assimilation without perturbed observations. *Mon. Wea. Rev.,* **130,** 1913–1924.

——, G. P. Compo, X. Wei, and T. M. Hamill, 2004: Reanalysis without radiosondes using ensemble data assimilation. *Mon. Wea. Rev.,* **132,** 1190–1200.

Wu, B., J. Verlinde, and J. Sun, 2000: Dynamical and microphysical retrievals from Doppler radar observations of a deep convective cloud. *J. Atmos. Sci.,* **57,** 262–283.

Xue, M., M. Tong, and K. K. Droegemeier, 2005: Impact of radar configuration and scan strategy on assimilation of radar data using ensemble Kalman filter. Preprints, *Ninth Symp. on Integrated Observing and Assimilation Systems for the Atmosphere, Oceans, and Land Surface,* San Diego, CA, Amer. Meteor. Soc., 9.3. [Available online at http://ams.confex.com/ams/pdfpapers/86681.pdf.]

——, ——, and ——, 2006: An OSSE framework based on the ensemble square-root Kalman filter for evaluating impact of data from radar networks on thunderstorm analysis and forecast. *J. Atmos. Oceanic Technol.,* **23,** 46–66.

——, Y. Jung, and G. Zhang, 2007: Error modeling of simulated reflectivity observations for ensemble Kalman filter data assimilation of convective storms. *Geophys. Res. Lett.,* **34,** L10802, doi:10.1029/2007GL029945.